

Evolution of star clusters on eccentric orbits

Maxwell Xu Cai (蔡栩)^{1,2★†} Mark Gieles^{3†} Douglas C. Heggie⁴ and Anna Lisa Varri⁴

¹National Astronomical Observatories of China, Chinese Academy of Sciences, 20A Datun Rd, Chaoyang District, Beijing 100012, P. R. China

²Kavli Institute for Astronomy and Astrophysics, Peking University, Yi He Yuan Lu 5, Haidian District, Beijing 100871, P. R. China

³Department of Physics, University of Surrey, Guildford GU2 7XH, UK

⁴School of Mathematics and Maxwell Institute for Mathematical Sciences, University of Edinburgh, Kings Buildings, Edinburgh EH9-3JZ, UK

Accepted 2015 October 5. Received 2015 September 29; in original form 2015 August 3

ABSTRACT

We study the evolution of star clusters on circular and eccentric orbits using direct N -body simulations. We model clusters with initially $N = 8k$ and $16k$ single stars of the same mass, orbiting around a point-mass galaxy. For each orbital eccentricity that we consider, we find the apogalactic radius at which the cluster has the same lifetime as the cluster with the same N on a circular orbit. We show that then, the evolution of bound particle number and half-mass radius is approximately independent of eccentricity. Secondly, when we scale our results to orbits with the same semimajor axis, we find that the lifetimes are, to first order, independent of eccentricity. When the results of Baumgardt and Makino for a singular isothermal halo are scaled in the same way, the lifetime is again independent of eccentricity to first order, suggesting that this result is independent of the galactic mass profile. From both sets of simulations, we empirically derive the higher order dependence of the lifetime on eccentricity. Our results serve as benchmark for theoretical studies of the escape rate from clusters on eccentric orbits. Finally, our results can be useful for generative models for cold streams and cluster evolution models that are confined to spherical symmetry and/or time-independent tides, such as Fokker–Planck models, Monte Carlo models, and (fast) semi-analytic models.

Key words: methods: numerical – galaxies: star clusters: general.

1 INTRODUCTION

The evolution of star clusters is driven by internal factors, such as two-body relaxation, stellar and binary evolution, and external factors such as the galactic tidal field (see e.g. Heggie & Hut 2003). As a result, star clusters gradually dissolve and eventually lose all their stars to the galactic field.

The escape rate from clusters in a static tidal field, as applies to cluster on circular orbits in a time-independent external potential, has been topic of extensive theoretical (e.g. Hénon 1961; King 1966; Gieles, Heggie & Zhao 2011) and numerical work (e.g. Chernoff & Weinberg 1990; Oh & Lin 1992). A consensus picture for the dependence of the dissolution time-scale τ_{diss} on the properties of the cluster and its orbit has emerged.

When approximating the tidal limitation by a simple cut-off radius, beyond which stars are considered unbound, τ_{diss} scales with the half-mass relaxation time-scale τ_{rh} of the cluster, which itself depends on the number of stars in the cluster N , the crossing time of stars within the cluster τ_{cr} as $\tau_{\text{rh}} \propto (N/\log \Lambda)\tau_{\text{cr}}$, where $\log \Lambda$ is the Coulomb logarithm, which slowly varies with N . For Roche-filling

clusters on circular orbits in a scale-free galactic potential, τ_{cr} is a constant fraction of the period of the galactic orbit, hence for these clusters $\tau_{\text{cr}} \propto \Omega^{-1}$ (Lee & Ostriker 1987), with Ω the angular frequency of the orbit.

If a tidal field is included, the escape of stars is delayed (Fukushige & Heggie 2000), and this effect changes the N dependence of τ_{diss} to (Baumgardt 2001)

$$\tau_{\text{diss}}(R_G, \epsilon = 0) \propto \left(\frac{N}{\log \Lambda} \right)^{3/4} \Omega^{-1}. \quad (1)$$

Here, ϵ is the orbital eccentricity and R_G is the galactocentric radius, which for the circular orbit relates to Ω as $\Omega = V_{\text{circ}}/R_G$, with V_{circ} the circular velocity at R_G .

For compact clusters that underfill the Roche volume, the fraction of escapers per τ_{rh} is lower because the tides are weaker, and because τ_{rh} itself is shorter, the fraction of escapers per unit of physical time is approximately independent of the half-mass radius r_h of the cluster and the result for τ_{diss} of equation (1) is, therefore, almost independent of the initial r_h (Gieles & Baumgardt 2008).

Baumgardt & Makino (2003, hereafter BM03) studied clusters on circular and eccentric orbits using direct N -body integrations with NBODY4 (Aarseth 1999). Their clusters contained a stellar mass spectrum, the effect of stellar and binary evolution and a realistic description of the tidal field of the galaxy, which was assumed to be

*Also known as: Maxwell Tsai.

†E-mail: maxwell@nao.cas.cn (MXC); m.gieles@surrey.ac.uk (MG)

due to a singular isothermal galactic halo. For eccentric orbits, they find that the N dependence in τ_{diss} is the same as for the circular orbits, and they show that τ_{diss} can be expressed in terms of the scaling for the circular orbits as

$$\tau_{\text{diss}}(R_a = R_G, \epsilon) = \tau_{\text{diss}}(R_G, 0)(1 - \epsilon). \quad (2)$$

Here R_a is the apogalactic radius of the orbit, which in [BM03](#) was kept the same as the galactocentric radius R_G of the circular orbit.

Along an eccentric orbit, the tidal field strength varies and it is, therefore, often assumed that the evolution of clusters on eccentric orbits is determined by the perigalactic radius R_p , where the tidal field is strongest ([King 1962](#); [Innanen, Harris & Webbink 1983](#)). This is indeed true for collisionless systems ([Peñarrubia, Navarro & McConnachie 2008](#)), but it is not what follows from the [BM03](#) result for collisional systems on eccentric orbits. Taken together, equations (1) and (2) suggest that the ‘effective radius’ R_G^{eff} , i.e. the radius of the circular orbit on which a cluster has the same lifetime as a cluster on the given elliptic orbit, is given by $R_G^{\text{eff}} = R_p(1 + \epsilon) = R_a(1 - \epsilon)$, i.e. the effective radius lies between R_p and R_a . The different dependence of τ_{diss} on the external tides as compared to the collisionless case, suggests that the combined influence of two-body relaxation and the (time-dependent) tides, result in a different overall evolution of (globular) clusters than what is found for (collisionless) dwarf galaxies that get tidally stripped in the host potential (see also the discussion in [Amorisco 2015](#), on differences in the escape mechanisms in collisional and collisionless systems).

In this study, we want to establish whether it is possible to approximate the evolution of a cluster on an eccentric orbit, by that of a cluster on a circular orbit. Whether possible, or not, the answer helps to identify the dominant mechanism that drives the escape from clusters on eccentric orbits. If possible, it would greatly simplify the treatment of eccentric orbits in dynamical models of cluster evolution that are limited to spherical symmetry/circular orbits and in (fast) semi-analytic models of clusters and cold tidal streams. Secondly, we aim to shed light on the scaling for $\tau_{\text{diss}}(R_a, \epsilon)$ for clusters on eccentric orbits.

We run a series of direct N -body integrations of idealized systems, without the effect of stellar evolution, which can be scaled and compared to the result of [BM03](#). This paper is organized as follows: the details of the N -body experiments are described in Section 2. Our results are presented in Section 3 and our conclusions are presented in Section 4.

2 N-BODY SIMULATIONS

2.1 N-body integrator and units

For all simulations, we used the N -body code `NBODY6`, which is a fourth-order Hermite integrator with [Ahmad & Cohen \(1973\)](#) neighbour scheme ([Makino & Aarseth 1992](#); [Aarseth 1999, 2003](#)), with accelerated force calculation on `NVIDIA` Graphical Processing Units (GPUs; [Nitadori & Aarseth 2012](#)). All our models are scaled to the conventional Hénon N -body units ([Hénon 1971](#)), in which $G = M = -4E = 1$, where G is the gravitational constant and M and E are the total mass and energy of the cluster, respectively. Our models are initially in virial equilibrium, such that the gravitational energy $W = 2E$ and the virial radius $r_v = -GM^2/(2W) = 1$.

2.2 Initial conditions

We model clusters with $N = 8\text{k}$ and 16k point particles of the same mass, without primordial binaries, with initial positions and velocities sampled from a [Plummer \(1911\)](#) model, truncated at 10 scale radii.¹ For this model, $r_h \simeq 0.78r_v$. The galactic potential is that of a point mass and the differential forces due to the galaxy are added in a non-rotating frame that is initially centred on the centre of mass of the cluster.

We adopt this simplified set of initial conditions because (i) we want to focus on one single physical ingredient (i.e. the tidal field), explored within the simplest possible choice of galactic mass model, (ii) some of the key results of the paper are based on three different scaling of the simulations, which must therefore be performed in the absence of any factor imposing a physical scale (e.g. stellar evolution), (iii) we wish to provide some ‘empirical’ evidence of the process underlying the escape of stars from clusters on elliptic orbits, for which a proper theory is still lacking, therefore we decided to explore first very idealized models, and to increase the complexity of the systems under consideration only in a second phase of the investigation.

For each N , we consider seven different orbital eccentricities: $\epsilon = [0.0, 0.1, 0.2, 0.3, 0.4, 0.6, 0.8]$. For the circular orbits, we choose an orbit such that $r_h/r_j = 0.1$, where r_j is the Jacobi radius, which for the point-mass galaxy and $\epsilon = 0$ depends on R_G and the mass of the galaxy M_G as

$$r_j = \left(\frac{M}{3M_G} \right)^{1/3} R_G. \quad (3)$$

The initial conditions of `NBODY6` need to be fed in physical units. We choose $M_G = 10^{10} M_\odot$, $r_v = 1$ pc and $\bar{m} = M/N = 1 M_\odot$. The remaining parameter to choose is R_G , which given the constraint of the initial r_h/r_j and equation (3) is $R_G = 7.86(3 \times 10^{10}/N)^{1/3}$ pc, which is $R_G = 1211$ pc (962 pc) for the circular orbit of the $N = 8\text{k}(16\text{k})$ cluster.² All models started with the same $r_h = 0.78$ in N -body units. The physical units are only used in the input of the code, and they are not relevant for our results and we report all our results in the internal N -body units (Section 2.1).

We define τ_{diss} as the time when 10 per cent of the initial number of stars remains bound. We then need to define bound. For a cluster on a circular orbit, in a coordinate system centred on the cluster and corotating with the galactic orbit, bound is defined as having a Jacobi energy smaller than the critical energy of escape. For eccentric orbits, there is no conserved integral of motion; hence, we need to find another way to separate bound from unbound stars. We consider a star as bound when the sum of its specific kinetic energy, computed from the velocities corrected for the centre-of-mass velocity, is less than its specific potential energy due to the $N - 1$ other stars, with N being determined iteratively until convergence (as in [Renaud, Gieles & Boily 2011](#)).

For each value of ϵ we aim to find the R_a that results in the same τ_{diss} as for the circular orbit at R_G , i.e. $\tau_{\text{diss}}(R_a, \epsilon) = \tau_{\text{diss}}(R_G, 0)$. This is different from the approach of [BM03](#), who started all

¹ In principle, the Plummer model has no truncation radius; in practice, it is truncated at 10 scale radii in `NBODY6`.

² In this paper, we use the definition of $1\text{k} = 1000$, so that the 8 and 16k models correspond to the total particle number of exactly 8000 and 16 000, respectively. Note that this is slightly different from the convention used in the [BM03](#) paper, where they defined $1\text{k} = 1024$.

Table 1. Apogalactic radii R_a for the $N = 8k$ and $16k$ simulations that result in the same τ_{diss} as the circular model. The values of R_a for each ϵ were found by iteration, see the text in Section 2.2 for details.

N	τ_{diss}	$R_a(\epsilon)$						
		0	0.1	0.2	0.3	0.4	0.6	0.8
8k	5060	1212	1362	1516	1798	2043	2934	4834
16k	8230	962	1081	1245	1420	1677	2502	4126

their eccentric orbits at the same $R_a(\epsilon) = R_G(\epsilon = 0)$, which results in shorter lifetimes for the eccentric orbits. In Section 3, we scale results for comparison. Because we do not know the scaling of $R_a(R_G, \epsilon)$ a priori for clusters with the same r_h , we find R_a by iteration: in the first attempt, we adopt the scaling of BM03 (equation 2) and run a model with $R_a = R_G/(1 - \epsilon)^{2/3}$ (note that the index of $2/3$ is because for a point-mass galaxy $\Omega \propto R_G^{-3/2}$). At this stage we could adapt the scaling $\tau_{\text{diss}}(R_a) \propto R_a^{-3/2}$ to find R_a that results in the correct lifetime. However, scaling will not keep the initial half-mass radius fixed, which is our intention in this study, and we therefore proceed by finding the correct R_a by iteration.

If τ_{diss} of the first attempt is shorter (longer) than that of the circular orbits, we run an additional model with R_a 20 per cent larger (smaller). We continue this, until we have two models whose $\tau_{\text{diss}}(R_a, \epsilon)$ bracket the result for the circular orbit. We then apply a linear interpolation to get the final R_a and run a model at that R_a . The final interpolated R_a values are summarized in Table 1.

The corresponding initial r_h/r_j at apocentre for all models with different orbital eccentricities ϵ are shown in Fig. 1, where r_j was computed using equation 7 in King (1962). For comparison, we present also the ratio r_h/r_j the cluster would have if we would have started the evolution at pericentre. We also show the values for r_h/r_j of the $N = 32k$ models of BM03, which we will later compare our results against, using the King (1962) definition for r_j (note that the equation used by BM03 is slightly different).

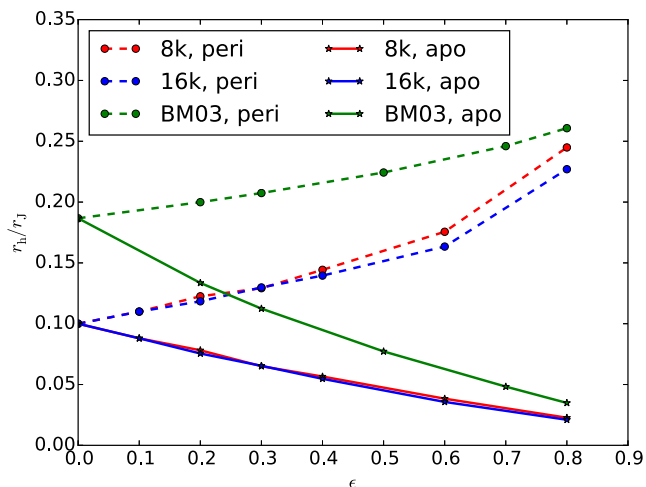


Figure 1. Initial r_h/r_j for all models as a function of orbital eccentricities ϵ . the values corresponding to the apocentre are connected with full lines; the values corresponding to the pericentre are connected with dashed lines. Results for the $N = 32k$ models of BM03 are also plotted in the same way for comparison.

3 RESULTS

3.1 Evolution of N and r_h : can the evolution on an eccentric orbit be compared to the evolution on a circular orbit?

Figs 2 and 3 show the evolution of the bound N for our models with different ϵ and initial $N = 8k$ and $16k$, respectively. The $N(T)$ curves of the models on eccentric orbits display a ‘staircase’ shape, with a frequency that corresponds to the orbital period. The amplitude of the ‘stairs’ depends on the number of particles N and the orbital eccentricity ϵ . The steps correspond to pericentre, where stars are removed fastest, and the fractional number of escapers at each step is larger in the small- N model because of two effects: (i) the lifetime of the small- N model is smaller (Figs 2 and 3), while (ii) the time between pericentre passages in the small- N model (which can be inferred from the values of R_a in Table 1) is larger. Therefore, the number of pericentre passages is smaller in the small- N model than in the corresponding large- N model. The rapid mass loss during the pericentre passages implies that dissolution is almost bound to happen around the pericentre, and for this reason the dissolution time of the high-eccentricity models is not really a continuous function of ϵ . This is important to keep in mind for the forthcoming comparison of lifetimes for different N .

We note that the removal of stars at pericentre does not imply that pericentre crossings are the sole mechanism that unbinds stars. For alternative definitions of bound, for example, being within r_j , the $N(T)$ curves display an oscillating behaviour, where $N(T)$ goes

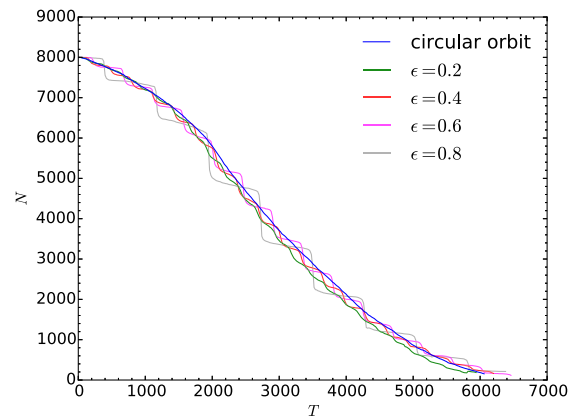


Figure 2. Evolution of the number of bound stars for the 8k models with different orbital eccentricities ϵ .

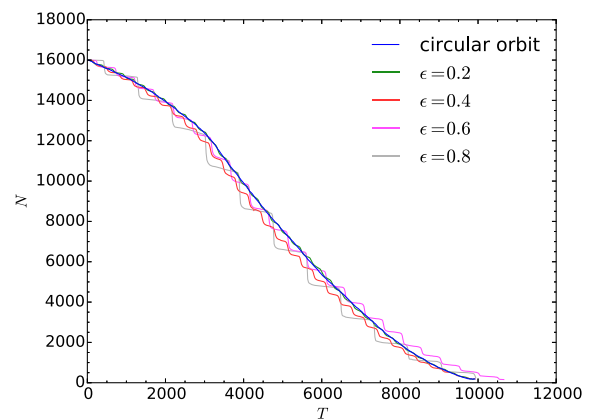


Figure 3. Evolution of number of bound stars for the 16k models with different orbital eccentricities ϵ .

up after a pericentre passage (see e.g. fig. 2 in BM03). This should also not be interpreted as mass gain of the cluster. Both the staircase pattern, and the oscillations, are artefacts of the definition of bound for clusters and illustrate that it is not possible to have a unique definition of the number of bound stars in a cluster on an eccentric orbit. However, the differences between $N(T)$ for different definitions of bound are small and it is safe to interpret the general trend of $N(T)$ as the evolution of the number of stars in the cluster.

Comparing the overall shape of the $N(T)$ curves of the different orbits, we see that there are similarities. Core collapse is reached at approximately $T = 0.3\tau_{\text{diss}}$, after which the escape rate approximately doubles (Lamers, Baumgardt & Gieles 2010). For equal-mass models without mass-loss as the result of stellar evolution, the escape rate increases in the pre-collapse phase and this manifests in all curves as a convex curvature (a negative second derivative). After core collapse the escape rate goes as $\dot{N} \propto N^{1/4}$ (equation 1, and Baumgardt 2001), which manifests as a concave curve $N(T)$ (positive second derivative, note that a constant \dot{N} would result in linear $N(T)$ curves). The curvature in pre-collapse and post-collapse evolution is similar for models of different ϵ , though it may be complicated by the ‘steps’ caused by pericentre passages. This trend is not known to apply universally for all galactic tidal fields, but a discussion of the shapes of $N(t)$ curves is beyond the scope of this paper.

In Figs 4 and 5, we show the evolution of $r_h(T)$ of the bound stars for the $N = 8k$ and $16k$ models, respectively. As for the $N(T)$,

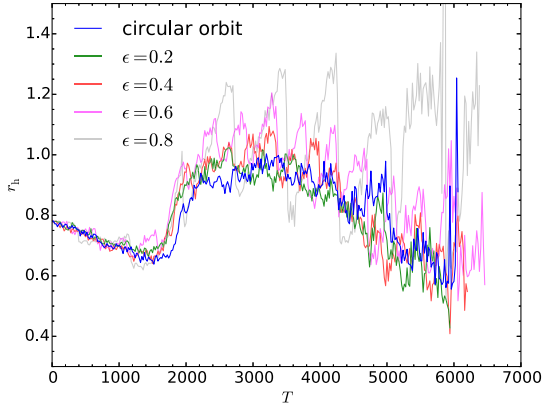


Figure 4. Half-mass radius r_h evolution of the 8k models with different ϵ and the same τ_{diss} .

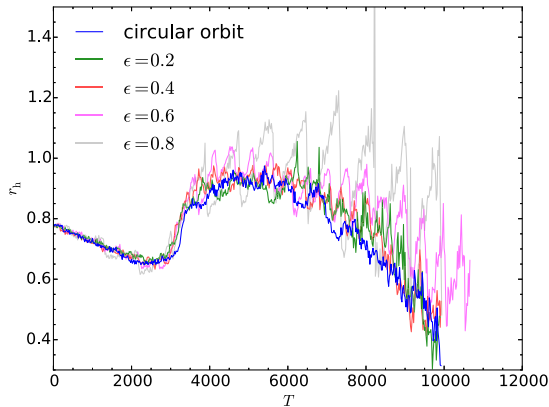


Figure 5. Same as Fig. 4 but for 16k models.

there is general agreement in shape of the $r_h(T)$ curves. All models start with the same initial $r_h \simeq 0.78$, and until core collapse, r_h shrinks as the result of escapers and the absence of a central energy source (Gieles et al. 2014). During the gravothermal catastrophe, r_h increases by about 50 per cent, after which it gradually decreases as $N^{1/3}$ (Hénon 1961). Similar to the $N(T)$ curves, the $r_h(T)$ curves also exhibit oscillation behaviour and the amplitudes depend on both N and ϵ . During pericentre r_h decreases sharply and then slowly grows until the next pericentre. We note that this behaviour depends on our definition of bound. For example, r_h of all the stars within r_j also oscillates, but has a maximum at R_a .

We recognize similar overall behaviour of $r_h(T)$ in all models, and combined with the similarity between the $N(T)$ curves, we conclude that it is possible to describe the evolution of a cluster on an eccentric orbit, by the evolution of a cluster on a circular orbit with the same τ_{diss} .

3.2 Scaling of $\tau_{\text{diss}}(R_a, \epsilon)$

3.2.1 Results for constant τ_{diss}

In Fig. 6, we show the ratio of $R_a(\epsilon)$ (Table 1) over $R_a(0) = R_G$ of the circular orbit, for all ϵ considered. For constant R_a , τ_{diss} must be a decreasing function of ϵ , and so for increasing ϵ , R_a must increase to keep τ_{diss} of the eccentric orbit the same as the circular orbit, and this is indeed what we find. The way $R_a(\epsilon)$ increases with increasing ϵ contains information about how τ_{diss} depends on ϵ .

In a forthcoming study, Bar-Or et al. (in preparation) derive the dependence of τ_{diss} on ϵ using perturbation theory. They find that, to first order, τ_{diss} is independent of ϵ for orbits with the same semi-major axis a (Bar-Or, private communication). To test this result we plot a line $R_a(\epsilon) = R_a(0)(1 + \epsilon)$, corresponding to orbits with the same a , because $R_a(\epsilon) = a(1 + \epsilon)$ and for the circular orbit $R_G = a$. We see that this relation follows the results of our simulations for $\epsilon \lesssim 0.3$ quite well, independently of N , and confirming the first order result of Bar-Or et al. (in preparation). But we also consider eccentricities that are much higher than the regime to which the perturbation theory applies. These empirical results thus serve to quantify the higher order dependence of $\tau_{\text{diss}}(a, \epsilon)$ on ϵ , which is the topic of the next sections.

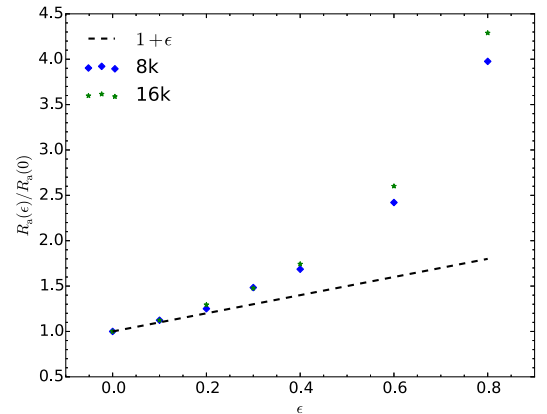


Figure 6. The apocentre distance $R_a(\epsilon)$, normalized to $R_a(0)$ of the circular orbit, for clusters with the same lifetimes and different eccentricities ϵ (data from Table 1). To first order the data follows the relation $y = 1 + \epsilon$, corresponding to a constant semimajor axis a .

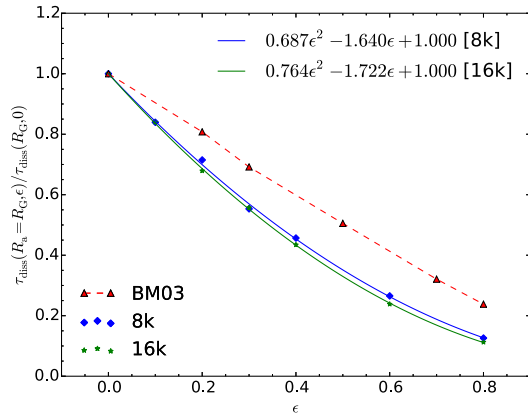


Figure 7. Dissolution times for all models scaled to the same R_a , normalized to τ_{diss} of the circular orbit. Solid lines denote polynomial fits to the data (for details, see Section 3.2.2). Also shown are the results for the $N = 32k$ models of **BM03**.

3.2.2 Results scaled to constant R_a

We first want to directly compare our results to the scaling for $\tau_{\text{diss}}(R_a, \epsilon)$ reported by **BM03** (equation 2). To make the comparison, we need to scale our results such that all our models have the same R_a . We, therefore, need to multiply all our galactic radii by a scale factor $R_* = R_a(0)/R_a(\epsilon)$. Because for the point-mass galaxy the radial scale of the cluster is proportional to the galactic radial scale (equation 3), the scale factor for the cluster’s length scale is $r_* = R_*$ and the scale factor for time can be related to the galactic scale factor as $t_* = R_*^{3/2}$. In Fig. 7, we show the results for τ_{diss} scaled to the same R_a , combined with the results of **BM03**. The ϵ dependence seems to be stronger in our models, which is suggestive that the mass profile of the galaxy is important in setting $\tau_{\text{diss}}(\epsilon)$.

However, the difference can be understood (at least for small ϵ) by adopting the hypothesis that τ_{diss} is independent of ϵ for fixed $a = R_G$, as in Section 3.2.1, i.e. that $\tau_{\text{diss}}(R_a = R_G(1 + \epsilon), \epsilon) = \tau_{\text{diss}}(R_G, 0)$. Since $t_* = R_*^{3/2}$ for the point-mass galaxy, we deduce that $\tau_{\text{diss}}(R_a = R_G, \epsilon) = \tau_{\text{diss}}(R_G, 0)/(1 + \epsilon)^{3/2} \simeq \tau_{\text{diss}}(R_G, 0)(1 - 1.5\epsilon)$. For the singular isothermal model of **BM03**, however, $t_* = R_*$, and so the corresponding result is $\tau_{\text{diss}}(R_a = R_G, \epsilon) \simeq \tau_{\text{diss}}(R_G, 0)(1 - \epsilon)$. Our hypothesis therefore explains why the dependence on ϵ in Fig. 7 is steeper for our models than in **BM03**, for small ϵ , and unifies the results of the two studies in this regime.

Fig. 7 also gives second-order polynomial fits³ to our results, and the foregoing argument approximately explains the first-order coefficient of ϵ in these fits. **BM03** themselves showed that the factor $1 - \epsilon$ gave a satisfactory fit to their models for the entire range of ϵ . By reversing the above argument we easily see that this result is consistent with a hypothesis that $\tau_{\text{diss}}(R_a = R_G(1 + \epsilon), \epsilon) = \tau_{\text{diss}}(R_G, 0)(1 - \epsilon^2)$, which we discuss further in the next section, where we scale all results to orbits with the same a .

3.2.3 Results scaled to constant semimajor axis a

To be able to compare all results to the theoretical prediction by Bar-Or et al. (in preparation), we present all results scaled to orbits

³ It could be argued that the lifetime should be zero for $\epsilon = 1$, and the quadratic fits provided in Fig. 7 are inconsistent with this, but those in Fig. 8 accommodate this idea. On the other hand, the lifetime of the model can hardly be less than the time taken to reach perigalacticon.

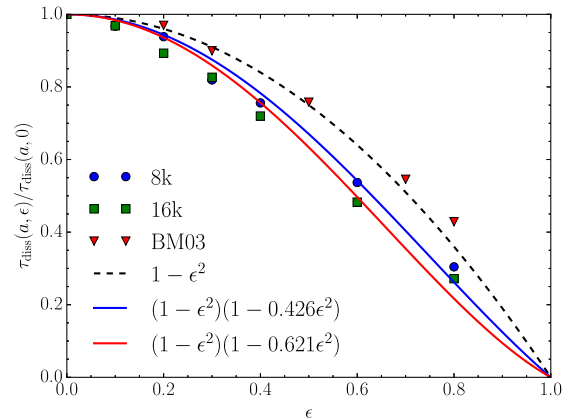


Figure 8. Dissolution time τ_{diss} for different ϵ , normalized to the result for the circular orbit, for the models discussed in this paper and **BM03** (32k models). All results have been scaled to orbits with the same semimajor axis a . Simple even polynomial functions, up to fourth order in ϵ , are shown for comparison (for details, see Section 3.2.3).

with the same a . We note that the results of this exercise for the **BM03** models should be interpreted with caution, because their models include the effect of stellar evolution, which imposes a fixed physical time-scale. Bearing this word of caution in mind, we scale the galactic orbits with $R_* = (1 + \epsilon)R_a(0)/R_a(\epsilon)$. The radial scale factor of the cluster itself is dependent on the mass profile: for the point-mass galaxy $r_* = R_*$ as before, while for the singular isothermal halo $r_* = R_*^{2/3}$. The scale factors for time for the two galaxy mass models are related to R_* as $t_* = R_*^{3/2}$ and $t_* = R_*$, respectively.

In Fig. 8, we present the results of all models, scaled to the same a and normalized to the circular orbit. We note that Webb et al. (2014) studied eccentric orbits with direct N -body models with similar properties as **BM03**, and they compared a model with high eccentricity ($\epsilon = 0.9$) to a model on a circular orbit with approximately the same lifetime. Applying the same scaling to their values of R_a we find that their $\epsilon = 0.9$ data point would extend the trend of the **BM03** scaling. Our results are slightly below the results of **BM03**. It is tempting to explain this offset to the difference in galactic mass model: the point-mass model has stronger tidal forces at peri-centre and, therefore, one way of interpreting the difference in Fig. 8 is that clusters on eccentric orbits dissolve faster in such haloes.

However, the small difference can perhaps also be explained by differences in how the clusters were setup relative to the tides and the differences in treatment of stellar evolution. **BM03** consider King models with Roche-filling initial conditions for the models on circular orbits, which means that the truncation radius of the King model equals r_J . For their models on circular orbits the initial ratio $r_h/r_J \simeq 0.19$ (Fig. 1), which is somewhat larger than what is adopted here ($r_h/r_J = 0.1$).

In addition, their models consider stellar evolution mass loss, and for the clusters on circular orbits, a fraction of the stars is pushed over the tidal boundary as the result of the expansion due to stellar mass loss (Lamers et al. 2010), shortening the lifetimes of the models on circular orbits by a mechanism that is not included in our models (for a discussion on the sensitivity of the Roche-filling models of **BM03** to stellar mass-loss, see Contenta, Varri & Heggie 2015).

For eccentric orbits, **BM03** fix r_h to the value a cluster would have on a circular orbit at R_p of the eccentric orbit. During the evolution,

r_j is time dependent, but motivated by our earlier finding, we can define r_j for the eccentric orbit as the Jacobi radius of an identical cluster on a circular orbit with the same τ_{diss} . Using that definition, the **BM03** models initially have $r_h/r_j \propto (1 + \epsilon)^{-2/3}$, whereas in our models $r_h/r_j = 0.1$, for all ϵ . Therefore, the **BM03** models with high ϵ are more compact with respect to the tides than our models, which could result in slightly larger τ_{diss} compared to our models at the same ϵ . We are therefore cautious with interpreting the small difference between the **BM03** results, and ours, as being due to difference in galactic mass profile.

In order to quantify the higher order dependence of τ_{diss} on ϵ , we plot two simple functions in Fig. 8. The functional form $y = 1 - \epsilon^2$ is motivated by the results of **BM03**, because this relation is what follows when scaling the result reported by **BM03** (equation 2) to orbits with constant a (Section 3.2.2). As expected, this relation describes the **BM03** results very well. However, it overpredicts τ_{diss} of our models, with a maximum difference of about 20 per cent at $\epsilon = 0.6$.

Motivated by our empirical findings, and the theoretical work of Bar-Or et al. (in preparation), we speculatively propose a characterization of the higher order dependence of τ_{diss} on ϵ , on the basis of a simple symmetry argument. Indeed, it can be argued that the quantity $\tau_{\text{diss}}(a, \epsilon)/\tau_{\text{diss}}(a, 0)$ should naturally be an even function of ϵ , which implies that, in a series expansion in ϵ , the odd terms of any order must vanish. This expectation on the parity of the function follows if we assume that the lifetime is independent of the initial phase on the galactic orbit, as reversing the sign of ϵ simply corresponds to starting at perigalacticon instead of (as in our models) at apogalacticon. We therefore consider an even, polynomial function such that $y(\epsilon) = 0$ for $\epsilon = 1$: $y(x) = (1 - \epsilon^2)(1 + (c + 1)\epsilon^2)$, in which the constant term is imposed to be 1 by virtue of the chosen normalization $\tau_{\text{diss}}(a, \epsilon)/\tau_{\text{diss}}(a, 0)$. We have then determined the best-fitting value of the free coefficient c for the two sets of models with $N = 8\text{k}$ and 16k , as depicted in Fig. 8.

In consideration of the simplicity of our argument, based on a reasonable but unproven assumption, we encourage the reader to accept the values resulting from the fitting process only for empirical guidance, as the full perturbation analysis of the escape problem, which is needed to constrain analytically the coefficient c , is beyond the scope of this article (see Bar-Or et al., in preparation).

In addition, given the relatively low N of our models compared to the **BM03** simulations, and other differences in the initial conditions between the two sets of models (see the discussion above on differences in the initial r_h/r_j), we are cautious with concluding that these different scalings as being due to the different galactic mass models.

These results serve as benchmarks for future theoretical work on the dissolution of clusters on eccentric orbits in different galactic potentials.

4 CONCLUSIONS

We model star clusters on circular and eccentric orbits with direct N -body simulations in order to gain insight in the evolution of cluster properties at different eccentricities ϵ , and the scaling relations for the dissolution time-scale (τ_{diss}) as a function of ϵ . We deploy direct N -body simulations to model idealized systems of $N = 8\text{k}$ and 16k stars of the same mass, on orbits around a point-mass galaxy. For the models on eccentric orbits, we iteratively find the apogalactic radius R_a on which the cluster τ_{diss} is the same as for the circular orbit.

When scaling our results to orbits with the same semi-major axis a , we find that τ_{diss} is, to first order, independent of ϵ . We show that this scaling agrees with results presented by **BM03**, who modelled clusters with a mass spectrum and the effects of stellar mass loss in singular isothermal galactic haloes. Their results suggest slightly longer τ_{diss} at higher ϵ than found here, which can be explained by differences in the initial r_h with respect to the tidal truncation. Alternatively, there may be a dependence on galactic mass profile, in the sense that τ_{diss} is more sensitive to ϵ in the case of point-mass galaxies. This explanation has theoretical support, because the heating at perigalactic passages in a point-mass model is more severe than in the extended singular isothermal model (Gnedin, Hernquist & Ostriker 1999). Because of the many differences between our models and the **BM03** we are cautious with interpreting the small difference between our results and **BM03** in either direction.

Finally, we quantify the higher order dependence of $\tau_{\text{diss}}(a, \epsilon)$ on ϵ . A relation of the form $\tau_{\text{diss}}(a, \epsilon) = f(\epsilon)\tau_{\text{diss}}(a, 0)$, with $f(\epsilon) = 1 - \epsilon^2$ describes the results of **BM03** very well. For the models presented here, a functional form of $f(\epsilon) = (1 - \epsilon^2)(1 - c\epsilon^2)$, with $c \simeq 0.5$, is more accurate. These data serve as benchmark for future theoretical work on the dissolution of clusters on eccentric orbits.

We find that clusters with the same initial N , r_h and τ_{diss} , but different ϵ , have similar evolution of the number of bound stars and half-mass radius r_h . This implies that we can approximate the evolution of properties of clusters on eccentric orbits by that of clusters on circular orbits. This is useful for modelling techniques that are not able to include orbital eccentricity, such as the Fokker–Planck method, or the Monte Carlo method and/or time-dependent galactic tides. For example, Heggie & Giersz (2008) present Monte Carlo models of the galactic globular cluster M4, which is on an eccentric orbit. The authors model M4 on a circular orbit, with approximately the same τ_{diss} as M4 has on its eccentric orbit. Our results confirm that this approach is valid and results in a representative evolution of N and r_h in these models. Another application of our result can be found in semi-analytic models of cluster evolution (e.g. Gnedin, Ostriker & Tremaine 2014). The fast cluster evolution code Evolve Me A Cluster of StarS (*EMACSS*; Alexander & Gieles 2012; Gieles et al. 2014; Alexander et al. 2014) solves a set of coupled differential equations for the rate of change of r_h , r_j and N . The method requires an expression for \dot{N} that depends on the tidal field. The results in this study can be used to include orbital eccentricity in *EMACSS* by using the functional form for $\tau_{\text{diss}}(a, \epsilon)$ to include ϵ in the \dot{N} term.

Finally, several models for generating tidal tails of globular clusters have recently been developed (Küpper, Lane & Heggie 2012; Bovy 2014; Amorisco 2015). These models require as input an escape rate of stars from the cluster. Our analytic expression for $\tau_{\text{diss}}(a, \epsilon)$ can be used to obtain expressions for the average escape rate from clusters on eccentric orbits.

ACKNOWLEDGEMENTS

We wish to thank the anonymous referee for her/his comments that helped to improve the manuscript considerably. This work was initiated during the International Summer-Institute for Modeling in Astrophysics (ISIMA) in 2014, hosted at CITA at the University of Toronto. We gratefully thank the organizers of ISIMA, especially Pascale Garaud, for the kind support of our participation. We thank CITA for hosting the ISIMA programme. We thank Florent Renaud, Rainer Spurzem and Thijs Kouwenhoven for useful discussions. MXC acknowledges supported by Chinese Academy

of Sciences Grant Number 2009S1-5, and through the ‘Thousand Talents’ (Qianren) programme of China (R. Spurzem). MG acknowledges financial support from the Royal Society (University Research Fellowship) and the European Research Council (ERC-StG-335936, CLUSTERS), and ALV from the Royal Commission for the Exhibition of 1851. All authors are grateful to Keigo Nitadori and Sverre Aarseth for making `NBODY6` and its GPU-enabled version publicly available and to Dave Munro of the University of Surrey for his support of the GPU cluster at the University of Surrey.

REFERENCES

- Aarseth S. J., 1999, *PASP*, 111, 1333
Aarseth S. J., 2003, *Gravitational N-Body Simulations*. Cambridge Univ. Press, Cambridge
Ahmad A., Cohen L., 1973, *J. Comput. Phys.*, 12, 389
Alexander P. E. R., Gieles M., 2012, *MNRAS*, 422, 3415
Alexander P. E. R., Gieles M., Lamers H. J. G. L. M., Baumgardt H., 2014, *MNRAS*, 442, 1265
Amorisco N. C., 2015, *MNRAS*, 450, 575
Baumgardt H., 2001, *MNRAS*, 325, 1323
Baumgardt H., Makino J., 2003, *MNRAS*, 340, 227 (BM03)
Bovy J., 2014, *ApJ*, 795, 95
Chernoff D. F., Weinberg M. D., 1990, *ApJ*, 351, 121
Contenta F., Varri A. L., Heggie D. C., 2015, *MNRAS*, 449, L100
Fukushige T., Heggie D. C., 2000, *MNRAS*, 318, 753
Gieles M., Baumgardt H., 2008, *MNRAS*, 389, L28
Gieles M., Heggie D. C., Zhao H., 2011, *MNRAS*, 413, 2509
Gieles M., Alexander P. E. R., Lamers H. J. G. L. M., Baumgardt H., 2014, *MNRAS*, 437, 916
Gnedin O. Y., Hernquist L., Ostriker J. P., 1999, *ApJ*, 514, 109
Gnedin O. Y., Ostriker J. P., Tremaine S., 2014, *ApJ*, 785, 71
Heggie D. C., Giersz M., 2008, *MNRAS*, 389, 1858
Heggie D., Hut P., 2003, eds, *The Gravitational Million-Body Problem: A Multidisciplinary Approach to Star Cluster Dynamics*. Cambridge Univ. Press, Cambridge, p. 372
Hénon M., 1961, *Ann. Astrophys.*, 24, 369
Hénon M. H., 1971, *Ap&SS*, 14, 151
Innanen K. A., Harris W. E., Webbink R. F., 1983, *AJ*, 88, 338
King I., 1962, *AJ*, 67, 471
King I. R., 1966, *AJ*, 71, 64
Küpper A. H. W., Kroupa P., Baumgardt H., Heggie D. C., 2010, *MNRAS*, 407, 2241
Küpper A. H. W., Lane R. R., Heggie D. C., 2012, *MNRAS*, 420, 2700
Lamers H. J. G. L. M., Baumgardt H., Gieles M., 2010, *MNRAS*, 409, 305
Lee H. M., Ostriker J. P., 1987, *ApJ*, 322, 123
Makino J., Aarseth S. J., 1992, *PASJ*, 44, 141
Nitadori K., Aarseth S. J., 2012, *MNRAS*, 424, 545
Oh K. S., Lin D. N. C., 1992, *ApJ*, 386, 519
Peñarrubia J., Navarro J. F., McConnachie A. W., 2008, *ApJ*, 673, 226
Plummer H. C., 1911, *MNRAS*, 71, 460
Renaud F., Gieles M., Boily C. M., 2011, *MNRAS*, 418, 759
Webb J. J., Leigh N., Sills A., Harris W. E., Hurley J. R., 2014, *MNRAS*, 442, 1569

This paper has been typeset from a $\text{T}_{\text{E}}\text{X}/\text{L}_{\text{A}}\text{T}_{\text{E}}\text{X}$ file prepared by the author.